ACS OMEGA

http://pubs.acs.org/journal/acsodf

Article

Preparation of Fetal Bovine Serum−Copper Phosphate Hybrid Particles under Cell Culture Conditions for Cancer Cell Treatment

Chihiro Mochizuki, Junna Nakamura, and Michihiro Nakamura*

Cite This: *ACS Omega* 2022, 7, 29495−29501

Read Online

ACCESS | Metrics & More | Article Recommendations | Supporting Information

ABSTRACT: Fetal bovine serum (FBS) particles, which mainly consist of bovine serum albumin, have the potential for biological and medical applications as drug carriers. The coacervation of albumin is a common technique for preparing albumin-based particles. The replacement of salt with novel metal salts such as Cu is an affordable way to embed the metal ion in the albumin-based particles. Further, increased Cu distribution is prevalent in many cancers. Here, we prepared adhesive cell-like FBS−copper phosphate hybrid particles [FBS-$Cu_3(PO_4)_2$], which exhibited toxicity toward cancer cells, with a narrow size distribution under cell culture conditions for preventing tumor progression. FBS-$Cu_3(PO_4)_2$ showed peroxidase-like activity. In addition, FBS-$Cu_3(PO_4)_2$ was successfully loaded with rhodamine B and conjugated with fluorescein isothiocyanate as models of drugs by coincubation. Thus, we designed a simple preparation method for optimizing FBS-$Cu_3(PO_4)_2$ synthesis under cell culture conditions. FBS-$Cu_3(PO_4)_2$ has significant potential as an efficient reactive oxygen species generator and drug-delivery agent against cancer cells. Furthermore, the RhoB-loaded FBS-$Cu_3(PO_4)_2$ successfully interacted with 4T1 mouse mammary tumor cells and were confirmed to exhibit toxicity.

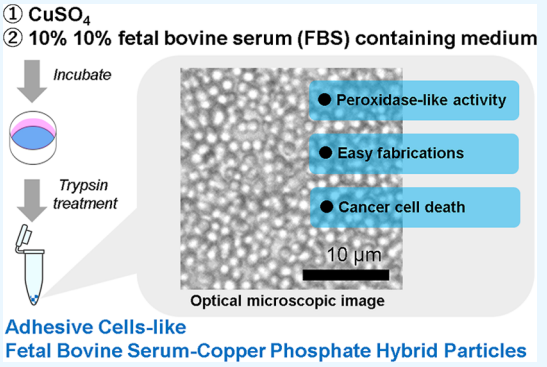

INTRODUCTION

The biological origin of fetal bovine serum (FBS) particles affords them biodegradability, nontoxicity, nonimmunogenicity, and easy availability. Bovine serum albumin (BSA) is the major component of FBS and has been widely used in medical applications.[1] Generally, albumin-based particles are prepared by coacervation methods such as desolvation.[2] It has been reported that adding alcohols, such as ethanol, and salts to the albumin water phase induces phase separation by desolvation.[3] The replacement of salt with novel metal salts such as Cu is an attractive way to embed the metal ion in the albumin-based particles. Further, Cu is an essential element in biological systems. Several types of cancers exhibit increased intratumoral and altered systemic Cu distribution.[4] Thus, two approaches for combating cancer have been investigated: (1) the development of copper-specific chelators to prevent tumor progression, including growth, angiogenesis, and metastasis because Cu serves as a limiting factor for multiple aspects of tumor progression and angiogenesis growth and so forth[5] and (2) delivering Cu, which possesses anticancer properties, to cancer cells because of the increased intracellular Cu levels in cancer cells.[6] From the perspective of reactive oxygen species (ROS) generation, Cu-containing catalysts have garnered considerable attention.[7] Recently, some studies have reported that metal-containing catalysts of peroxidase mimic the chemical catalytic reaction that decomposes H_2O_2 into the highly toxic hydroxyl radical ($^{\bullet}OH$).[8,9] In biological systems, Cu-based ROS generation may amplify the therapeutic effect in the tumor tissue compared to the normal tissue. Using various proteins and Cu(II), protein−inorganic hybrid nanoflowers have been synthesized. They were formed by the coordination of copper phosphate [$Cu_3(PO_4)_2$] and amide groups in the protein.[10] This has led to studies on protein−inorganic hybrid flowers that demonstrate high enzyme activity for the biosensor and the catalyst.[11−14]

In this study, we prepared adhesive cell-like FBS-$Cu_3(PO_4)_2$ particles under cell culture conditions. The cell culture conditions are widely established for in vitro experiments; thus, this preparation method of FBS-$Cu_3(PO_4)_2$ would widely spread as an easy and convenient way for anti-cancer materials in the biology laboratory. Optical microscopy revealed high transparency and narrow distribution of the particles. FBS-$Cu_3(PO_4)_2$ also showed peroxidase-like activity. Further, the FBS-$Cu_3(PO_4)_2$ particles were successfully loaded with rhodamine B (RhoB) and conjugated with fluorescein isothiocyanate (FITC) by coincubation. The RhoB-loaded FBS-$Cu_3(PO_4)_2$ successfully interacted with 4T1 mouse mammary tumor cells and were confirmed to be toxic. This report

Received: June 29, 2022
Accepted: August 3, 2022
Published: August 12, 2022

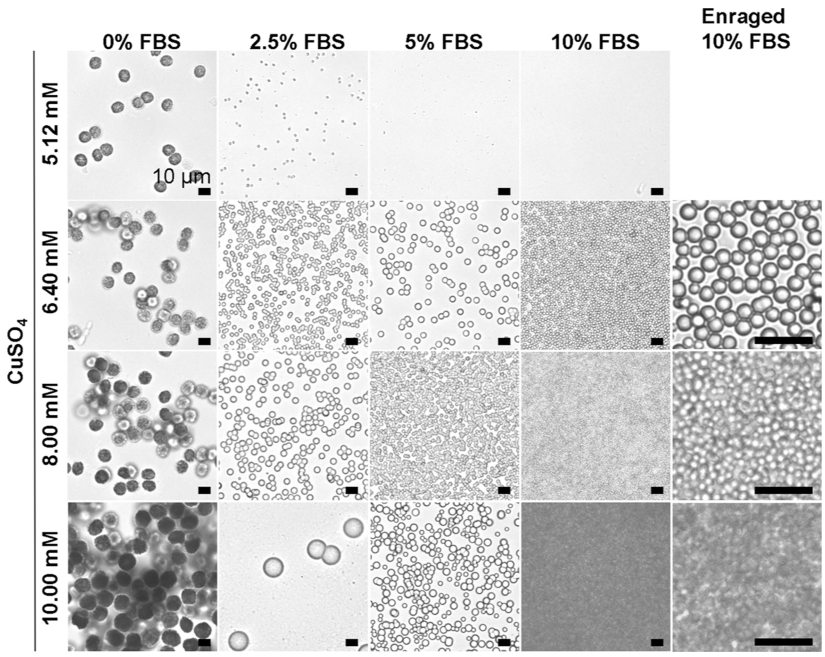

Figure 1. Optical microscopy images of FBS-$Cu_3(PO_4)_2$ in different concentrations of FBS and $CuSO_4$. Scale bar = 10 μm.

presents a simple preparation method for optimizing the fabrication of FBS-$Cu_3(PO_4)_2$ under cell culture conditions. FBS-$Cu_3(PO_4)_2$ has potential as an efficient ROS generator and drug-delivery agent against cancer cells.

RESULTS AND DISCUSSION

Preparation and Characterization of FBS-$Cu_3(PO_4)_2$. We successfully prepared FBS-$Cu_3(PO_4)_2$ determined by optical and electron microscopies under cell culture conditions.

Optical Microscopic Observation. Figure 1 and Table 1 show the optical microscopy images and the effect of FBS and $CuSO_4$ concentrations on the diameter of FBS-$Cu_3(PO_4)_2$. Initially, we focused on the effect of $CuSO_4$ concentration at a constant FBS concentration. At 0% FBS, the diameter of $Cu_3(PO_4)_2$ increased slightly as the $CuSO_4$ concentration increased from 5.12 to 10.00 mM. It has been reported that the initial Cu concentration slightly affects the diameter of precipitated Cu(II) hydrous oxide particles.[15] With increasing Cu concentration (5.12−10.00 mM), the diameter of FBS-$Cu_3(PO_4)_2$ increased at 2.5% FBS but decreased at 10% FBS. The diameter demonstrates opposite trends at low and high concentrations of FBS, suggesting the difference in the formation mechanism.[16] Figure S1 shows the optical microscopy images under different conditions without the Roswell Park Memorial Institute (RPMI) (+/+) medium. With 0% FBS in phosphate-buffered saline (PBS) (−), the particles were formed, and at 10% FBS in PBS (−), the particles formed, but were primarily inhomogeneous, suggesting that RPMI (+/+) contributed to the preparation of highly monodisperse FBS-$Cu_3(PO_4)_2$.

Table 1. Effect of the Reaction Condition on the Size of FBS-$Cu_3(PO_4)_2$

conditions		characterization
FBS (% (w/w))	Cu (mM)	diameter (nm)[a]
0.0	5.12	9.9 ± 0.5
0.0	6.40	9.9 ± 0.6
0.0	8.00	10.5 ± 0.5
0.0	10.00	12.5 ± 2.0
2.5	5.12	1.9 ± 0.4
2.5	6.40	3.5 ± 0.3
2.5	8.00	5.7 ± 0.2
2.5	10.00	14.6 ± 4.2[b]
5.0	5.12	no formation
5.0	6.40	5.5 ± 0.4
5.0	8.00	3.0 ± 0.5
5.0	10.00	5.1 ± 1.2
10.0	5.12	no formation
10.0	6.40	2.1 ± 0.3
10.0	8.00	1.0 ± 0.2
10.0	10.00	unmeasurable

[a]Average diameters and S.D.s of FBS-$Cu_3(PO_4)_2$ determined by optical microscopic images were calculated from more than 50 particles for each sample. [b]Less than 50 particles (formation of particles was less).

Electron Microscopy. Figure 2 shows the electron microscopy images of FBS-$Cu_3(PO_4)_2$ washed with PBS (−) and those after protein decomposition of FBS-$Cu_3(PO_4)_2$. In the former, at 0% FBS, FBS-$Cu_3(PO_4)_2$ formed a flowerlike structure,[12,13] whereas at 2.5, 5, and 10% FBS, it formed a spherical shape with a more smooth surface compared to the previously reported petal structure of hybrid nanoflowers composed of BSA and $Cu_3(PO_4)_2$.[10] After protein decomposition at 0 and 2.5% FBS, flowerlike structures were observed, suggesting that the nucleation growth of $Cu_3(PO_4)_2$ was prioritized under these conditions. These results indicate that the trend of the diameter increase with increasing Cu concentration is caused by the crystallization of $Cu_3(PO_4)_2$ at low concentrations of FBS (Table 1). Conversely, at 5 and 10% FBS, the structure of $Cu_3(PO_4)_2$ was not observed; instead, a flat-shaped structure was observed in the scanning electron microscopy (SEM) images, which showed a high contrast in the scanning transmission electron microscopy (STEM) images. This implies that $Cu_3(PO_4)_2$ was

https://doi.org/10.1021/acsomega.2c04096
ACS Omega 2022, 7, 29495−29501

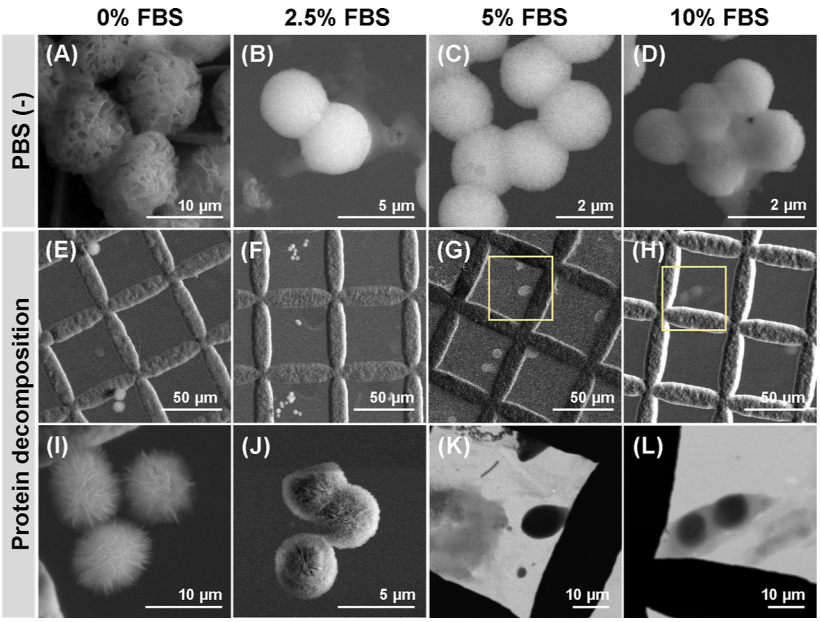

Figure 2. Electron microscopy images of FBS-$Cu_3(PO_4)_2$ at different concentrations of FBS. The concentration of $CuSO_4$ was fixed at 8.00 mM. Scale bars were inadvertently introduced into the figure. (A–D) FBS-$Cu_3(PO_4)_2$ was washed with PBS (−). (E–L) Protein of FBS-$Cu_3(PO_4)_2$ was decomposed using the cell lysis solution. (I,L) Enlarged SEM images. (K,L) Enlarged STEM images of the yellow parts of (G,H), respectively.

not crystallized, and FBS-$Cu_3(PO_4)_2$ was constructed by the coordination of FBS and $Cu_3(PO_4)_2$. Thus, the decreasing tendency of the diameter with the increasing Cu concentration at high FBS concentrations is caused by the coacervation of FBS by Cu(II) (Table 1).

Selected Electron Diffraction Patterns, FT-IR Spectroscopy, and TGA. Figure 3A shows the TEM images and selected electron diffraction patterns of FBS-$Cu_3(PO_4)_2$ for 0 and 10% FBS, namely, $Cu_3(PO_4)_2$ and FBS-$Cu_3(PO_4)_2$, respectively. $Cu_3(PO_4)_2$ showed numerous diffraction spots from multiple crystals representing a concentric ring, suggesting that $Cu_3(PO_4)_2$ particles prepared in 0% FBS are composed of multiple crystalline structures. Conversely, FBS-$Cu_3(PO_4)_2$ showed a slightly broad pattern, called the halo ring pattern, which is indicative of its amorphous phase structure.[17]

Figure 3B shows the Fourier transform infrared (FT-IR) spectra of $Cu_3(PO_4)_2$ and FBS-$Cu_3(PO_4)_2$. For $Cu_3(PO_4)_2$, the peak corresponding to the adsorbed water at 1635 cm^{-1} was observed. Additionally, the peaks at 1139, 1053, and 993 cm^{-1} correspond to the bending vibration of Cu−OH and asymmetric and symmetric stretching vibrations of PO_4^{3-}, respectively. The peaks at 624 and 561 cm^{-1} correspond to the out-of-plane bending vibrations of the PO_4^{3-} ions.[12,18] For FBS-$Cu_3(PO_4)_2$, characteristic peaks ascribed to proteins were observed at the amide I (1641 cm^{-1}, C═O stretching) and amide II (1541 cm^{-1}, overlap of N−H bending and C−N stretching) bands, suggesting the presence of proteins in FBS-$Cu_3(PO_4)_2$.[12,19] The peak at 1453 cm^{-1} may be attributed to the in-plane bending vibration of C−H and O−H bonds of the protein,[12] also suggesting the incorporation of proteins in FBS-$Cu_3(PO_4)_2$.

Figure 3C shows the thermogravimetric analysis (TGA) data for $Cu_3(PO_4)_2$ and FBS-$Cu_3(PO_4)_2$. The initial weight loss of $Cu_3(PO_4)_2$ and FBS-$Cu_3(PO_4)_2$ below 150 °C is associated with the loss of physically adsorbed water.[12,20] FBS-$Cu_3(PO_4)_2$ showed a weight loss at 150−350 °C, corresponding to the loss of low-molecular-weight compounds.[21] Above 350 °C, higher weight loss denoting the degradation of proteins originating from FBS and structurally bound water molecules occurred,[12,20] suggesting the presence of protein in FBS-$Cu_3(PO_4)_2$.

Peroxidase-like Activity of FBS-$Cu_3(PO_4)_2$. Figure 4A shows the peroxidase-like activity of FBS-$Cu_3(PO_4)_2$. As compared to natural peroxidase enzymes, artificial enzymes possess the advantages of controlled synthesis at a low cost and tunability during catalytic activities. We evaluated the oxidation of 3,3′,5,5′-tetramethylbenzidine (TMB) as a substrate into ox-TMB (deep blue color, with a maximum absorbance at 652 nm) in the presence of H_2O_2 by FBS-$Cu_3(PO_4)_2$. The absorbance (at 652 nm) increases as the concentration of FBS-$Cu_3(PO_4)_2$ increases. Figure 4B shows the time-dependent absorbance changes with 25 μg mL^{-1} FBS-$Cu_3(PO_4)_2$. An increase in absorbance is observed with time, which is indicative of the catalytic activity of FBS-$Cu_3(PO_4)_2$. In contrast, under the same reaction conditions, the absorbance did not increase in the absence of the particles.

Preparation and Characterization of RhoB-Loaded and FITC-Conjugated FBS-$Cu_3(PO_4)_2$. Albumin-based particles are commonly used for multiparticulate drug-delivery systems, owing to their advantage of broad functionalization, such as with organic compounds. We investigated two types of functionalization methods with organic compounds: RhoB for the loading method and FITC for the conjugation method were used as model drugs for observing and evaluating the drug-loading capacity (Figure 5A). RhoB and FITC were successfully embedded in FBS-$Cu_3(PO_4)_2$ with the diameters of 2.3 ± 0.3 nm and 3.0 ± 0.5 nm, respectively (Table S1). The diameter of FBS-$Cu_3(PO_4)_2$ was 1.0 ± 0.2 nm in the absence of the organic compound, suggesting that the addition of the organic compound in the reaction solution affected the size of FBS-$Cu_3(PO_4)_2$. The functionalization with organic compounds also affected the size of the particles. These particles fluoresced when observed under fluorescent microscopy. RhoB as a cationic compound could interact via

https://doi.org/10.1021/acsomega.2c04096
ACS Omega 2022, 7, 29495−29501

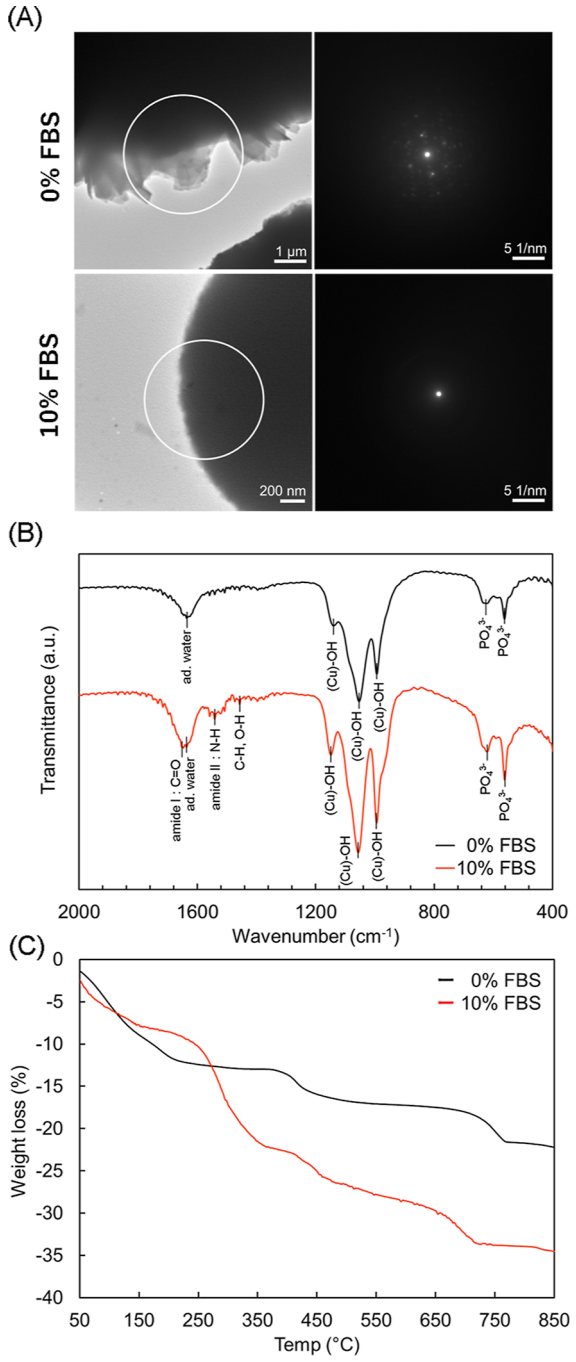

Figure 3. (a) Selected electron diffraction patterns, (b) FT-IR spectra, and (c) TGA of $Cu_3(PO_4)_2$ and FBS-$Cu_3(PO_4)_2$ at different concentrations of FBS (0 and 10%). The concentration of $CuSO_4$ was fixed at 8.00 mM.

electrostatic interactions with FBS because BSA has an isoelectric point near pH ≈ 4.8, that is, it is negatively charged. FITC interacted with the amino residues of albumin because FITC possesses isothiocyanate (−NCS) groups.[22]

Figure 5B shows the time-series of the fluorescent microscopy images of 4T1 cells coincubated with RhoB-loaded FBS-$Cu_3(PO_4)_2$ and in the absence of the particles. The zeta potential of the RhoB-loaded FBS-$Cu_3(PO_4)_2$ was −0.38 ± 0.56 mV [in PBS (−)], and this value shifted slightly toward the positive compared to the value −3.24 ± 0.19 mV [in PBS (−)] of FBS-$Cu_3(PO_4)_2$ (Table S2). The loading quantity of

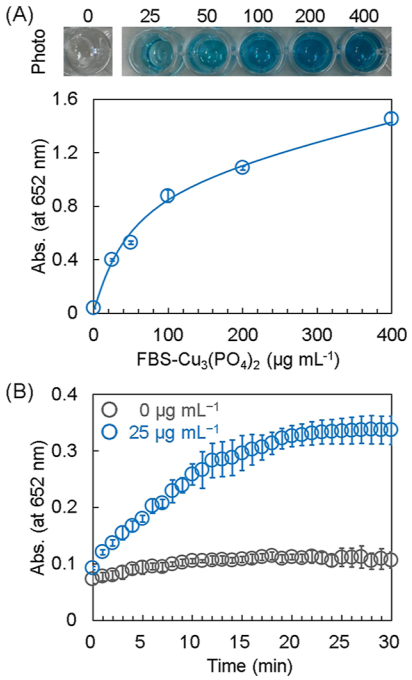

Figure 4. Peroxidase-like activity of FBS-$Cu_3(PO_4)_2$. (A) Dose-dependent absorbance changes at 652 nm. Reaction conditions; 0.8 mM TMB, 50 mM H_2O_2, 10 mM NaAc buffer (pH 5.0), FBS-$Cu_3(PO_4)_2$ = 0−400 μg mL^{-1} at 37 °C for 5 min. (B) Time-dependent absorbance changes at 652 nm of FBS-$Cu_3(PO_4)_2$. The preparation condition for FBS-$Cu_3(PO_4)_2$ was 10% FBS and 8.00 mM $CuSO_4$. Reaction conditions for peroxidase-like activity were 0.8 mM TMB, 50 mM H_2O_2, 10 mM NaAc buffer (pH 5.0), and FBS-$Cu_3(PO_4)_2$ = 0 and 25 μg mL^{-1} at 37 °C.

RhoB for FBS-$Cu_3(PO_4)_2$ was estimated from the fluorescent spectra measurements by FlexStation 3 (Figure S2); the number of RhoB that interacted with 1 mg of FBS-$Cu_3(PO_4)_2$ was 1.14×10^{23}. In Figure 5B, RhoB-loaded FBS-$Cu_3(PO_4)_2$ gradually interacted with the 4T1 cells as time progressed. After 12 h of coincubation, the greater part of RhoB-loaded FBS-$Cu_3(PO_4)_2$ interacted with the surface of the 4T1 cells, and the damaged 4T1 cell structure was observed after 24 h. In contrast, under identical incubation conditions, the 4T1 cells were not damaged in the absence of the particles. At a concentration of 25 μg mL^{-1}, FBS-$Cu_3(PO_4)_2$ reduced the viability of 4T1 cells to 5.7%, confirming its toxicity (see Supporting Information S3). These results indicate that RhoB-loaded FBS-$Cu_3(PO_4)_2$ showed toxicity on contact with the surface of 4T1 cells because of their peroxidase-like activity. Among the active oxygen species, H_2O_2 is relatively stable and can diffuse to longer distances.[23] Therefore, it is considered that peroxidase-like activity occurred actively on the cell surface, thereby causing oxidative damage to the cells.

CONCLUSIONS

We have successfully prepared adhesive cell-like FBS-$Cu_3(PO_4)_2$ hybrid particles and proposed a simple preparation method to optimize their synthesis under cell culture conditions. FBS-$Cu_3(PO_4)_2$ demonstrated peroxidase-like activity as an artificial enzyme and was easily functionalized with organic compounds as model drugs. Our results clearly demonstrate the potential of FBS-$Cu_3(PO_4)_2$ as an efficient ROS generator and drug-delivery agent for cancer cells. Therefore, FBS-$Cu_3(PO_4)_2$ is highly promising for medical

https://doi.org/10.1021/acsomega.2c04096
ACS Omega 2022, 7, 29495−29501

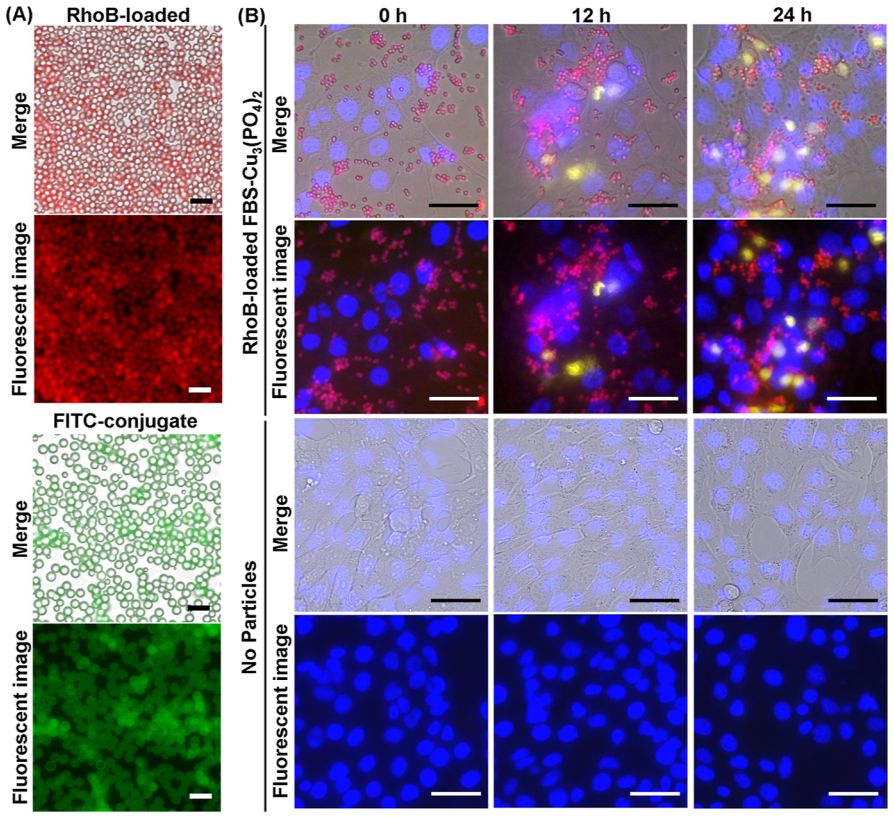

Figure 5. (A) Fluorescence microscopy images of RhoB-loaded and FITC-conjugate FBS-$Cu_3(PO_4)_2$. The preparation conditions for FBS-$Cu_3(PO_4)_2$ were 10% FBS, 8.00 mM $CuSO_4$, and 10 μM RhoB or FITC. The fluorescence of RhoB and FITC are represented in red (Ex: 545/25 nm, Em: 605/70 nm) and green (Ex: 470/40 nm, Em: 525/50 nm), respectively. Scale bar = 10 μm. (B) Time-series images of fluorescent microscopy of the 4T1 cells coincubated with RhoB-loaded $Cu_3(PO_4)_2$. The fluorescence of DAPI and Hoechst is represented in yellow (Ex: 360/40 nm, Em: 460/50 nm) and blue (Ex: 360/40 nm, Em: 460/50 nm), respectively. The 4T1 cells coincubated with RhoB-loaded FBS-$Cu_3(PO_4)_2$ and in the absence of the particles were first stained with DAPI and observed, followed by staining with Hoechst. Scale bar = 50 μm.

applications. Currently, a detailed study on its stability, drug release, and application in cancer therapy combined with radiotherapy for tumors is underway.

EXPERIMENTAL SECTION

Materials and Devices. Sulfate pentahydrate ($CuSO_4 \cdot 5H_2O$) was purchased from Wako Pure Chemical Industries, Japan. RhoB and FITC were purchased from Sigma-Aldrich. PBS solution was prepared as follows: 8.0 g of sodium chloride (NaCl), 0.2 g of potassium chloride (KCl), 0.2 g of sodium dihydrogen phosphate dehydrate ($NaH_2PO_4 \cdot 2H_2O$), and 2.9 g of disodium hydrogen phosphate dodecahydrate ($Na_2HPO_4 \cdot 12H_2O$) were mixed, and distilled water (DW) was added to make 1 L. The cell lysis solution was prepared as follows: 2 g of sodium deoxycholate, 2 g of sodium dodecyl sulfate, 2 mL of NP-40, and 37.2 mg of EDTA disodium salt were dissolved in 100 mL of DW.

Optical and fluorescent microscopy images were observed using a BZ-X800 fluorescence and light microscopy system (Keyence, Japan). SEM images were obtained using a Quanta 3D FEG electron microscope (FEI, Hillsboro, Oregon, USA) operated at 30 kV. TEM images were obtained via a JEM-2100 electron microscope (JEOL, Japan) operated at 200 kV. FT-IR spectra were recorded using an FT/IR-4600 spectrometer (JASCO, Tokyo, Japan). TGA was conducted on powdered samples using a HITACHI STA7200 (HITACHI, Japan) system from 30 to 900 °C at a heating rate of 10 °C min^{-1} under airflow at a rate of 200 mL min^{-1}.

Preparation of FBS-$Cu_3(PO_4)_2$. FBS-$Cu_3(PO_4)_2$ was prepared by adding 200 μL of the desired concentration of $CuSO_4$ in RPMI medium containing 0−10% heat-inactivated FBS and antibiotics (100 μg/mL streptomycin and 100 units/mL penicillin) in a well of black 96-well plates (Greiner Bio-One, USA). The mixture was incubated at 37 °C in a 5% CO_2 atmosphere for 2 d, yielding FBS-$Cu_3(PO_4)_2$ at the bottom of the well. In the presence of FBS, the FBS-$Cu_3(PO_4)_2$ adhered to the bottom of the well. The FBS-$Cu_3(PO_4)_2$ was washed with PBS (−) and collected using trypsin treatments. The suspended FBS-$Cu_3(PO_4)_2$ was centrifuged (1000*g*, 5 min) and purified by washing with PBS (−), and a blue FBS-$Cu_3(PO_4)_2$ precipitate was collected. The protein was decomposed using the cell lysis solution. The blue FBS-$Cu_3(PO_4)_2$ precipitate was mixed with the cell lysis solution at 37 °C for 30 min, centrifuged (1000*g*, 5 min), and purified by washing with PBS (−).

Peroxidase-like Activity of FBS-$Cu_3(PO_4)_2$. The peroxidase-like activity was induced by adding 400 μL of 10 mM buffer solution (NaAc, pH 5.0) in the order of certain amounts of FBS-$Cu_3(PO_4)_2$, 800 μM TMB, and 50 mM H_2O_2, yielding immediate color reactions.[8] After incubation at 37 °C for 5 min in the dark, the mixtures were immediately centrifuged (30,000*g*, 5 min). The supernatant was measured using a FlexStation 3 (Molecular Devices, USA) reader. Time-dependent absorbance changes were monitored using FlexStation 3 prior to centrifugation.

https://doi.org/10.1021/acsomega.2c04096
ACS Omega 2022, 7, 29495−29501

Preparation of RhoB-Loaded and FITC-Conjugated FBS-$Cu_3(PO_4)_2$. RhoB-loaded and FITC-conjugated FBS-$Cu_3(PO_4)_2$ particles were prepared by adding 200 μL of 8.00 mM $CuSO_4$ in RPMI medium containing 10% heat-inactivated FBS and antibiotics (100 μg/mL streptomycin and 100 units/mL penicillin) and RhoB and FITC adjusted to 10 μM, respectively, in a well of black 96-well plates (Greiner Bio-One, North Carolina). The mixture was incubated at 37 °C for 2 d. The RhoB-loaded and FITC-conjugated FBS-$Cu_3(PO_4)_2$ particles were washed with PBS (−) and collected using trypsin treatments. The suspended FBS-$Cu_3(PO_4)_2$ particles were centrifuged (1000*g*, 5 min) and purified by washing with PBS (−).

Cell Viability Assay Using WST-1. The viabilities of 4T1 cells were evaluated using the WST-1 cell proliferation reagent (Roche, Almere, Netherlands). The cells were seeded at a density of 1.0×10^4 cells/well in 96-well plates 24 h prior to being treated with FBS-$Cu_3(PO_4)_2$. The cells were incubated with 0−100 μg mL^{-1} of FBS-$Cu_3(PO_4)_2$ in Dulbecco's modified Eagle's medium (DMEM) containing 10% heat-inactivated FBS and antibiotics (100 μg mL^{-1} streptomycin and 100 units/mL penicillin) for 1 d at 37 °C. The absorbance of FBS-$Cu_3(PO_4)_2$ coincubated solution was immediately measured, following the addition of the WST-1 reagent and incubation at 37 °C. To isolate the signals that were derived from the formazan dye (produced by viable cells), the former signal was subtracted from the latter.

Observation of 4T1 Cells Using RhoB-Loaded FBS-$Cu_3(PO_4)_2$. 4T1 cells were cultured overnight at 37 °C in a 5% CO_2 atmosphere in 96-well plates in DMEM containing 10% heat-inactivated FBS and antibiotics (100 μg mL^{-1} streptomycin and 100 units/mL penicillin). Then, 25 μg mL^{-1} FBS-$Cu_3(PO_4)_2$ was incubated in DMEM containing 10% heat-inactivated FBS and antibiotics (100 μg mL^{-1} streptomycin and 100 units/mL penicillin), and time-series images for 24 h at 37 °C in a 5% CO_2 atmosphere were obtained.

■ ASSOCIATED CONTENT

Supporting Information

The Supporting Information is available free of charge at https://pubs.acs.org/doi/10.1021/acsomega.2c04096.

Optical microscopic images of FBS-$Cu_3(PO_4)_2$ in PBS (−) and 10% FBS/PBS (−) and cytotoxicity assessments of FBS-$Cu_3(PO_4)_2$ for 4T1 cells (PDF)

■ AUTHOR INFORMATION

Corresponding Author

Michihiro Nakamura − *Department of Organ Anatomy & Nanomedicine, Graduate School of Medicine, Yamaguchi University, Ube, Yamaguchi 755-8505, Japan; Core Clusters for Research Initiatives of Yamaguchi University, Ube, Yamaguchi 755-8505, Japan;* orcid.org/0000-0002-9216-3215; Phone: +81-836-22-2202; Email: nakam@yamaguchi-u.ac.jp

Authors

Chihiro Mochizuki − *Department of Organ Anatomy & Nanomedicine, Graduate School of Medicine, Yamaguchi University, Ube, Yamaguchi 755-8505, Japan; Core Clusters for Research Initiatives of Yamaguchi University, Ube, Yamaguchi 755-8505, Japan*

Junna Nakamura − *Department of Organ Anatomy & Nanomedicine, Graduate School of Medicine, Yamaguchi University, Ube, Yamaguchi 755-8505, Japan; Core Clusters for Research Initiatives of Yamaguchi University, Ube, Yamaguchi 755-8505, Japan*

Complete contact information is available at: https://pubs.acs.org/10.1021/acsomega.2c04096

Author Contributions

C.M. performed the synthesis and characterization of FBS-$Cu_3(PO_4)_2$ and drafted the manuscript. J.N. performed the cell culture and cytotoxicity test. M.N. supervised this work.

Funding

This study was supported in part by JSPS KAKENHI [Grant-in-Aid for Early-Career Scientists (no. 20 K15322), Grant-in-Aid for Scientific Research (B) (no. 20H03625), and Grant-in-Aid for Scientific Research (C) (nos. 21500409, 25350530, and 16K01358)].

Notes

The authors declare no competing financial interest.

■ ACKNOWLEDGMENTS

We appreciate the assistance of Koichiro Yuki with the electron microscopy observations.

■ REFERENCES

(1) Gupta, P. K.; Hung, C. T.; Perrier, D. G. Albumin Microspheres. II. Effect of Stabilization Temperature on the Release of Adriamycin. *Int. J. Pharm.* **1986**, *33*, 147−153.

(2) Spada, A.; Emami, J.; Tuszynski, J. A.; Lavasanifar, A. The Uniqueness of Albumin as a Carrier in Nanodrug Delivery. *Mol. Pharm.* **2021**, *18*, 1862−1894.

(3) Jahanban-Esfahlan, A.; Dastmalchi, S.; Davaran, S. A Simple Improved Desolvation Method for the Rapid Preparation of Albumin Nanoparticles. *Int. J. Biol. Macromol.* **2016**, *91*, 703−709.

(4) Denoyer, D.; Masaldan, S.; La Fontaine, S.; Cater, M. A. Targeting copper in cancer therapy: 'Copper That Cancer'. *Metallomics* **2015**, *7*, 1459−1476.

(5) Yang, Y.; Tang, J.; Zhang, M.; Gu, Z.; Song, H.; Yang, Y.; Yu, C. Responsively Aggregatable Sub-6 Nm Nanochelators Induce Simultaneous Antiangiogenesis and Vascular Obstruction for Enhanced Tumor Vasculature Targeted Therapy. *Nano Lett.* **2019**, *19*, 7750−7759.

(6) Zhang, C.; Yan, L.; Wang, X.; Dong, X.; Zhou, R.; Gu, Z.; Zhao, Y. Tumor Microenvironment-Responsive Cu2(OH)PO4 Nanocrystals for Selective and Controllable Radiosentization via the X-ray-Triggered Fenton-like Reaction. *Nano Lett.* **2019**, *19*, 1749−1757.

(7) Gawande, M. B.; Goswami, A.; Felpin, F. X.; Asefa, T.; Huang, X.; Silva, R.; Zou, X.; Zboril, R.; Varma, R. S. Cu and Cu-Based Nanoparticles: Synthesis and Applications in Catalysis. *Chem. Rev.* **2016**, *116*, 3722−3811.

(8) Tao, Y.; Lin, Y.; Huang, Z.; Ren, J.; Qu, X. Incorporating Graphene Oxide and Gold Nanoclusters: A Synergistic Catalyst with Surprisingly High Peroxidase-like Activity over a Broad PH Range and Its Application for Cancer Cell Detection. *Adv. Mater.* **2013**, *25*, 2594−2599.

(9) Pacchin Tomanin, P.; Bhangu, S. K.; Caruso, F.; Cavalieri, F. Catalytically Active Copper Phosphate−Dextran Sulfate Microparticle Coatings for Bioanalyte Sensing. *Part. Part. Syst. Charact.* **2020**, *37*, 2000210.

(10) Ge, J.; Lei, J.; Zare, R. N. Protein-Inorganic Hybrid Nanoflowers. *Nat. Nanotechnol.* **2012**, *7*, 428−432.

(11) Sun, J.; Ge, J.; Liu, W.; Lan, M.; Zhang, H.; Wang, P.; Wang, Y.; Niu, Z. Multi-Enzyme Co-Embedded Organic-Inorganic Hybrid

Nanoflowers: Synthesis and Application as a Colorimetric Sensor. *Nanoscale* **2014**, *6*, 255−262.
(12) He, G.; Hu, W.; Li, C. M. Spontaneous Interfacial Reaction between Metallic Copper and PBS to Form Cupric Phosphate Nanoflower and Its Enzyme Hybrid with Enhanced Activity. *Colloids Surf., B* **2015**, *135*, 613−618.
(13) Luo, Y. K.; Song, F.; Wang, X. L.; Wang, Y. Z. Pure Copper Phosphate Nanostructures with Controlled Growth: A Versatile Support for Enzyme Immobilization. *CrystEngComm* **2017**, *19*, 2996−3002.
(14) Duan, L.; Wang, H.; Hou, J.; Zhang, Y.; Chen, V. A Facile, Bio-Inspired Synthetic Route toward Flower-like Copper Phosphate Crystals with High Specific Surface Area. *Mater. Lett.* **2015**, *161*, 601−604.
(15) Candal, R. J.; Regazzoni, A. E.; Blesa, M. A. Precipitation of Copper(II) Hydrous Oxides and Copper(II) Basic Salts. *J. Mater. Chem.* **1992**, *2*, 657−661.
(16) Thanh, N. T. K.; Maclean, N.; Mahiddine, S. Mechanisms of Nucleation and Growth of Nanoparticles in Solution. *Chem. Rev.* **2014**, *114*, 7610−7630.
(17) Zhao, W.; Zhong, G.; McDonald, M. J.; Gong, Z.; Liu, R.; Bai, J.; Yang, C.; Li, S.; Zhao, W.; Wang, H.; Fu, R.; Jiang, Z.; Yang, Y. $Cu_3(PO_4)_2$/C Composite as a High-Capacity Cathode Material for Rechargeable Na-Ion Batteries. *Nano Energy* **2016**, *27*, 420−429.
(18) Wu, X.; Shi, G. Fabrication of a Lotus-like Micro−Nanoscale Binary Structured Surface and Wettability Modulation from Super-hydrophilic to Superhydrophobic. *Nanotechnology* **2005**, *16*, 2056−2060.
(19) Bandekar, J. Amide Modes and Protein Conformation. *Biochim. Biophys. Acta, Protein Struct. Mol. Enzymol.* **1992**, *1120*, 123−143.
(20) Can, K.; Ozmen, M.; Ersoz, M. Immobilization of Albumin on Aminosilane Modified Superparamagnetic Magnetite Nanoparticles and Its Characterization. *Colloids Surf., B* **2009**, *71*, 154−159.
(21) Yang, H.; He, P.; Yin, Y.; Mao, Z.; Zhang, J.; Zhong, C.; Xie, T.; Wang, A. Succinic Anhydride-Based Chemical Modification Making Laccase@$Cu_3(PO_4)_2$ Hybrid Nanoflowers Robust in Removing Bisphenol A in Wastewater. *Bioprocess Biosyst. Eng.* **2021**, *44*, 2061−2073.
(22) Mochizuki, C.; Nakamura, J.; Nakamura, M. Development of Non-Porous Silica Nanoparticles towards Cancer Photo-Theranostics. *Biomedicines* **2021**, *9*, 73.
(23) Test, S. T.; Weiss, S. J. Quantitative and Temporal Characterization of the Extracellular H2O2 Pool Generated by Human Neutrophils. *J. Biol. Chem.* **1984**, *259*, 399−405.

https://doi.org/10.1021/acsomega.2c04096
ACS Omega 2022, 7, 29495−29501